# Internal Stress in High-Strength CuAg Conductor

K. Han, V. J. Toplosky, R. M. Niu, and J. Lu

***Abstract*—Resistive magnets with ultrahigh magnetic fields require composite conductors (almost all based on Cu) with optimized combinations of mechanical strength and electrical conductivity. In the fabrication of these conductors, the lower the melting point of the alloys, the easier they are to cast. Among conductors with melting points below the melting point of Cu, those of Cu-Ag achieve the highest mechanical strength. During cold-rolling, which is the final step for making these Cu-Ag conductors, small Ag precipitates elongate into a high density of fine Ag fibers, thus producing the high strength of the material. In this study, ultimate tensile strength values reached >850 MPa when composites were rolled to a reduction-in-thickness of >97% and spacing between fibers was reduced to less than 50 nm, generating high internal stresses. In these composites, the ratio of ultimate strength in the transverse direction to that in the longitudinal direction was about 1.13, indicating anisotropy. We speculate that such anisotropy in mechanical strength may lead to an internal-stress anisotropy at macroscale that could later complicate the manufacture of Bitter plates. In order to optimize the manufacturing process, we quantified the relationship between internal stress and strength anisotropy in Cu-24wt% Ag.**

***Index Terms*—Anisotropic properties, high-strength conductor, internal stress, mechanical strength, resistive magnet.**

## I. Introduction

THE development of high-field DC magnets depends on three factors: The generation of high power, the optimization of design, and the manufacture of high-strength conductors [1], [2], [3]. Because of the Lorentz force exerted on current-carrying conductors, the achievement of very high magnetic fields is ultimately limited by the mechanical strength of the conductors themselves [4]. To overcome this limit, the most straightforward approach is to use a conductor with sufficient conductivity to suppress Joule heating and sufficient mechanical strength to resist the stress generated by the Lorentz force [5], [6], [7]. Researchers have made significant progress in improving the mechanical strength of the conductors used in high-field magnets. Some of these conductors are copper-matrix composites in which reinforcement is achieved by "implanting" into the copper matrix a multitude of second-phase particles in the shape of spheres, whiskers, ribbons, or filaments [5], [6], [7], [8], [9], [10], [11]. One of the implanting approaches is to alloy Cu in liquid form and then to solidify the liquid to produce precipitates from the alloying elements [12], [13], [14], [15], [16], [17], [18], [19]. In our laboratory, for example, deformed Cu-24wt%Ag composites are commonly used as conductors for DC resistive magnets because they have both high strength and high conductivity. During casting, which is the first step in the manufacture of these composites, many small Ag precipitates emerge from the supersaturated solid solution of Cu-Ag. During the deformation that takes place after solidification, precipitate particles morph into the shape of whiskers, ribbons, or filaments, which then strengthen the Cu matrix without significantly reducing its electrical conductivity [20], [21].

In high-strength conductors used in our laboratory, second phase particles co-exist with the Cu matrix. The lattice misfit between the matrix and the particles is what generates shortwave internal stresses [6], [8], [9]. Deformation alters these internal stresses so that longwave internal stresses are introduced as well as the shortwave ones. In other words, longwave internal stresses are the result of deformation inhomogeneity.

Deformation also introduces preferred orientations of crystal structure (see Fig. 1) so that mechanical and electrical property anisotropy occurs [10]. We believe that this texture also leads to anisotropy in internal stresses, which in turn may complicate the later manufacture of conductors [4], [22], [23], [24], [25].

In Bitter magnets, one of the manufacture parameters is the size of the slit that is necessary for assembling the Bitter discs. We found discs that were out of specification (either too wide or too narrow) because of large internal stresses. In this paper, we investigate internal stresses in Cu-Ag composites and discuss the mitigation of these stresses during the fabrication of conductors.

## II. Experimental Methods

### A. Materials

We conducted our research on sheets of Cu-Ag (Ag content 24wt%) that had been rolled to a thickness of 0.67 mm. This material was formed in our laboratory into Bitter discs with both slits and holes—the slits to facilitate stacking and the holes to facilitate cooling. These discs were intended to be stacked together to function as solenoid coils in our DC resistive magnets. In some of these discs, however, we found that the holes were misaligned because the slits did not adhere to the prescribed 0.5 mm nominal width. Some of the slits were more than double the prescribed size, and others disappeared because their edges overlapped. The end result was discs that were so warped they were unusable.

Manuscript received 16 October 2023; revised 5 December 2023 and 8 January 2024; accepted 14 February 2024. Date of publication 28 February 2024; date of current version 7 March 2024. This work was supported by the NSF and State of Florida undertaken at National High Magnetic Field Laboratory under Grant DMR-1644779, Grant DMR-1938789, Grant DMR-2131790, and Grant DMR-2128556, and in part by Florida State University Research Foundation and Florida State. *(Corresponding author: K. Han.)*

The authors are with National High Magnetic Field Laboratory, Florida State University, Tallahassee, FL 32310 USA (e-mail: han@magnet.fsu.edu; toplosky@magnet.fsu.edu; rniu@magnet.fsu.edu; jun-lu@magnet.fsu.edu).

Color versions of one or more figures in this article are available at https://doi.org/10.1109/TASC.2024.3368396.

Digital Object Identifier 10.1109/TASC.2024.3368396

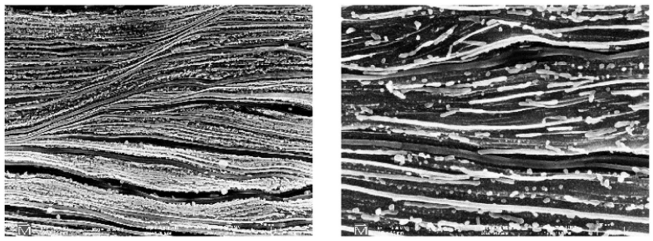

a. b.

Fig. 1. SEM images of longitudinal direction cross-section of a Cu-Ag plate. (a) Low magnification image showing Ag (bright contract) aligned in preferred orientation and shear band. (b) Large magnification image showing aligned Ag ribbons.

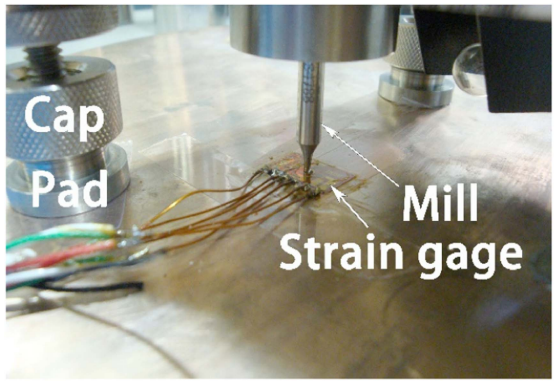


Fig. 2. Drilling of the central hole using a test fixture.

We speculated that the deformation process (which included both stamping and rolling) had introduced excessive residual stress.

### B. Mechanical Testing

Tensile tests were performed at room temperature (295 K) on a 100 kN MTS servo-hydraulic test system. Tensile test samples, which had been machined to a gauge length of 25 mm, were subjected to loading by the displacement-control method at a rate of 0.5 mm/min until failure. A 25 mm clip-on extensometer was used to record sample strain. Three samples were loaded in the Rolling Direction (RD) and three in the Transverse Direction (TD), which was perpendicular to the RD. Based on measured stress-strain curves, values were derived for Tensile Strength (TS) and Yield Strength (YS). (In this paper, TS is intended to refer to ultimate tensile strength; YS to 0.2% offset engineering flow stress.)

### C. Internal Stress Measurement

We measured residual stresses by a hole-drilling strain-gauge method that follows the ASTM standard E 837–94 [26]. Two rosette-style strain gauges from the Vishay Micro-Measurements group (No. CEA-06-062UL-120) were bonded to a 250 mm square sheet. Using the top-left corner as the 00 origin, the corner hole was located at $x = 30$ mm, $y = -50$ mm and the central hole was located at $x = 125$ mm and $y = -125$ mm (i.e., centrally located). The strain gauge rosette nominal diameter $D$ was measured to be 5.24 mm. The diameter of the drilled hole $D_o$ was 1.75 mm nominal, consistent with the drilled hole diameter based on the ASTM standard where $0.3 < (D_o/D) < 0.5$. According to the standard, for a material with a thickness that is less than $1.2D$ (as is the case of the 0.67 mm specimen), a hole passing through the entire thickness should be made. For the alignment and drilling of this hole, we used a Vishay Measurements Group Model RS-200 milling guide (see Fig. 2). We used a variable-speed electric hand drill to drive a 1/16th end mill. To maximize heat dissipation until the sample was drilled through, we performed the drilling by steps, each time increasing drilling depth by 0.076 mm. Prior to and after the drilling, strain values were measured by a Micro-Measurements D4 data acquisition conditioner.

After the drilling of each hole, the relieved strain parallel to the RD was measured as $\varepsilon_{\mathrm{L}}$. The strain 45 degrees to the RD was $\varepsilon_{45}$. The strain in the TD, which was perpendicular to the RD, was $\varepsilon_{\mathrm{T}}$. From these three strains, the angle ($\beta$) from the nearer principal axis to the RD, was calculated:

$$\beta \;=\; 1/2\,\tan^{-1}\left[\frac{\varepsilon_T + \varepsilon_L - 2\varepsilon_{45}}{\varepsilon_T - \varepsilon_L}\right] \tag{1}$$

The principal maximum stress $\sigma_{\max}$ was located clockwise (if positive) or counterclockwise (if negative) from the RD. Principal minimum stress $\sigma_{\min}$ was located at a $\beta$ measured clockwise from the TD. We calculated the values of $\sigma_{\max}$ (using $+$sign) and $\sigma_{\min}$ (using $-$sign) as follows:

$$\sigma_{\mathrm{man}}, \sigma_{\min} = \frac{\varepsilon_{\mathrm{T}} + \varepsilon_{\mathrm{L}}}{4\bar{A}} \pm \frac{\sqrt{(\varepsilon_L - \varepsilon_T)^2 + (\varepsilon_T + \varepsilon_L - 2\varepsilon_{45})^2}}{4\bar{B}} \tag{2}$$

where $\bar{A}$ and $\bar{B}$ are calibration constants and are dependent on the following material properties:

$$\bar{A} = -\left[(1+\mu)/2E\right]\bar{a} \tag{3}$$

$$\bar{B} \;=\; -\,(1/2\mathrm{E})\,\bar{b} \tag{4}$$

where E and μ are the Young's modulus and shear modulus, $\bar{a}$ and $\bar{b}$ are dimensionless coefficients that are dependent on strain gauge geometry. We took values $\bar{a}$ and $\bar{b}$ from Table II, reported in ASTM standard E 837–94 [26].

### D. Microstructure Examination

Samples were first wet-ground with 500 and 800 grit SiC paper and then polished with 9 and 3 μm polycrystalline diamond solutions. A final polish of 0.04 μm alumina particles in a slurry of approximately 9 pH was used on a vibrator polisher. The samples were then analyzed using a light microscope.

## III. Results

We determined that the distortion that occurs in the fabrication of Bitter discs is the direct result of anisotropy in the mechanical properties, the internal stresses, and the microstructure of the material.

TABLE I
MECHANICAL PROPERTIES OF CU-AG SHEETS

| Orientation | Modulus (GPa) | YS (MPa) | TS (MPa) | Elongation |
|---|---|---|---|---|
| RD | 108±3 | 780±10 | 875±1 | 4.6±0.2% |
| TD | 135±5 | 846±9 | 985±5 | 4.8±1.4% |
| TD/RD | 1.25 | 1.08 | 1.13 | 1.04 |

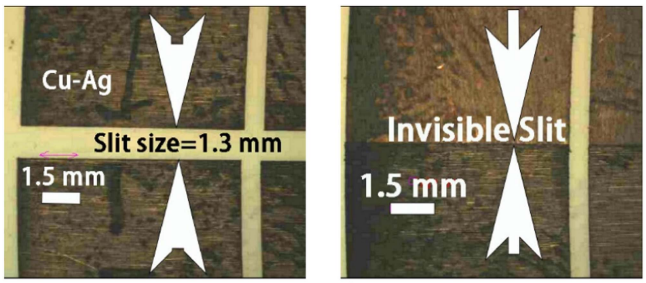


a. b.

Fig. 3. Two images at the same magnification showing slits in two discs after stamping. The slits are indicated by two arrows and oriented horizontally. (a) Slit is too wide; (b) Slit is too narrow.

### A. Mechanical Property Anisotropy

The ultimate Tensile Strength (TS) of our sheets in the TD ($TS_{TD}$) was higher than in the RD ($TS_{RD}$): $TS_{TD}/TS_{RD} = 1.13$:. A similar anisotropy was also reflected in the Youngs modulus and in the Yield Strength (YS, see Table I).

We observed anisotropy with respect to, not only the values for average TS, but also those for minimum TS. The minimum $TS_{RD}$ (874 MPa) was only marginally lower than the average $TS_{RD}$ but was much lower than the minimum $TS_{TD}$ (981 MPa), indicating marked anisotropy (see Table I).

The presence of anisotropy in major mechanical properties, which indicates internal stress anisotropy at macroscale, is one of the reasons why the width of the slits in Bitter discs often failed to meet our specifications.

### B. Distortion of Sheet Conductors

We noticed, when we first received our conductor sheets from the supplier, that some of them were warped. Then, after we had stamped these sheets (which measured $250 \times 250 \times 0.67$ mm$^3$ each) into donut-shaped discs with an outer diameter of 242 mm and an inner diameter of 141 mm, we noticed that, in about half of these discs, the slit was either too wide or too narrow (see Fig. 3). To learn whether these distortions had been introduced 1) by internal stress or 2) by warping in the original sheets or 3) by shear stress introduced into the discs during the process of stamping, we fastened some sheets onto a flat platform and then machined (rather than stamped) them into discs. In each disc, we then milled a slit $0.5 \pm 0.1$ mm wide. When we observed similar distortion in machined and milled discs, we concluded that the stamping process could not have been the cause of misalignment. The distortion must have been introduced into the original sheets by internal stress or warping that occurred during manufacture.

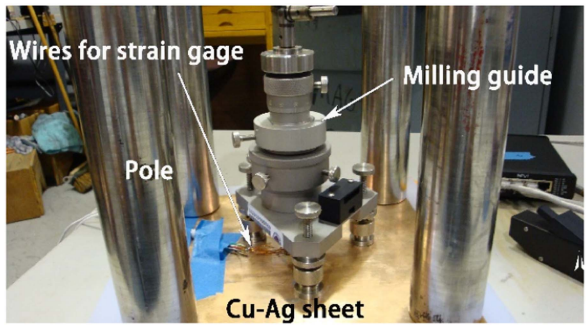


Fig. 4. Image showing the location of the posts and a sheet.

We estimated distortion strain as follows:

$$e = \delta l / \pi d \tag{5}$$

where e is the distortion strain, $\delta l$ is the difference between the final slit width and the designed slit width, and $d$ is the outer diameter of the disc. For a 1.5-mm-wide slit, for example, the strain value would be estimated as 0.105%. For a zero-mm-wide slit (i.e., no slit), the strain value would be estimated as $-0.067\%$.

Assuming that the distortion strain we observed resulted from elastic deformation, we used the average modulus shown in Table I to estimate residual stress values at 128 MPa for a 1.5-mm slit and $-80$ MPa for a zero-mm slit.

### C. Residual and Bending Stress

The initial condition, when all strain values were zero, was designated as Condition 1. In this condition, we had not yet drilled any hole in the disc, and we had not applied any pressure. Condition 2 was designated after a hole had been drilled. At this point, the residual stress values, $\sigma_{\max}$ and $\sigma_{\min}$, were both between 10 and 20 MPa, much lower than the residual stress values that we had estimated after the slit was first milled (128 MPa and $-80$ MPa, see section B above).

We recognized that bending strain should have been included in our original estimates. To simulate the bending stress that necessarily occurs during the process of fastening the materials for machining or stamping, we decided to use posts, each weighing 2.5 kg, to force the warped sheets to lie as flat as possible (see Fig. 4).

Condition 3 was designated after we had positioned three of these posts in order to flatten the sheet that had been drilled in Condition 2. We placed one post on each of three corners–bottom left, bottom right, and top right. We then measured 136 MPa for $\sigma_{\max}$ and $-3.32$ MPa for $\sigma_{\min}$. The value for $\sigma_{\max}$ was close to the residual stress value that we had estimated after the slit was first milled (see section B).

In Condition 4, the drill fixture was removed, and a fourth post was placed in the top left corner of the sheet. This caused the left side of the sample to lie flat while the bottom portion bowed convexly in the form of a bridge. The resulting $\sigma_{\max}$ and $\sigma_{\min}$ values were 191 MPa and $-4.3$ MPa, respectively. The value for $\sigma_{\min}$ was too small to be significant, but $\sigma_{\max}$ was about 1.5 times the stress level that had appeared in the sheet with the 1.5 mm slit (see Section B).

TABLE II
STRESS VALUES IN FIVE CONDITIONS

| Conditions | 1.5-mm slit | 2 | 3 | 4 | 5 |
|---|---|---|---|---|---|
| $\sigma_{max}$ (MPa) | 128 | <20 | 136 | 193 | 263 |
| $\sigma_{min}$ (MPa) | N/A | <10 | -3.3 | -4.3 | 33 |

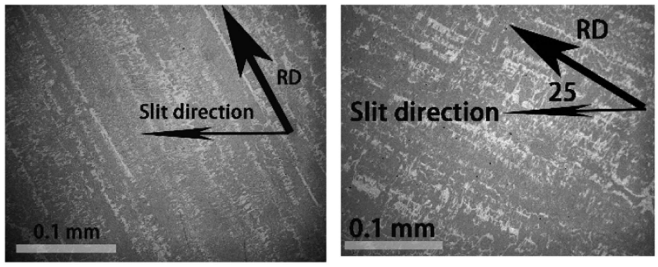


a. b.

Fig. 5. Light microscopy image showing slit orientation with respect to microstructure. The light-colored contrast in the microstructure indicates the presence of Ag. In these samples slits are oriented horizontally in the figure. (a) Sample with slit width of 0.5 +/− 0.1 mm. The angle between slit and rolling direction is about 60° and (b) The width of the slit is about 0.68 mm, i.e., 0.18 mm greater than desired specifications. The angle between slit and rolling direction is about 25°.

In Condition 5, we attempted to reduce bowing by applying light pressure to the bottom portion of the sheet. This pressure, however, only shifted the bowing from convex to concave, causing the left edge of the sample to bow upwards. The resulting $\sigma_{\max}$ and $\sigma_{\min}$ values were 263 MPa and 33 MPa, respectively. The $\sigma_{\min}$ was again too small to be significant, but the $\sigma_{\max}$ was now twice the stress level that had appeared in the sheet with the 1.5 mm slit above.

To summarize, Condition 3 produced the best description of the internal stress level that appeared in the sheet with the distorted slit (Table II). Slit distortion resulted from both internal stress (elastic in nature) and bending stress (plastic in nature).

### D. Microstructure and Internal Stress

Once discs had been fabricated from sheets, we could no longer identify the rolling direction. Consequently, we could not correlate the anisotropy of the microstructure and properties of the sheets with the slit distortion in the discs. We therefore sectioned, mounted, and polished certain Bitter discs in order to establish a relationship between microstructure and slit sizes.

In a Bitter disc with a slit size slightly smaller than 0.5 mm, the Ag phase appeared to be aligned about 60° from the slit orientation (see Fig. 5). This alignment was later confirmed to be the major rolling-line direction of the as-received sheets.

We estimated the circumference strain as ∼0.01% in a Bitter disc with a slit size about 0.18 mm larger than the designed width. The rolling direction (identified by the orientation of the Ag phase) appeared to be aligned about 25° from the slit orientation.

From the above data, we deduced that distortion was smaller in the width of a slit when the slit was aligned closer to the transversal direction (<25°).

## IV. DISCUSSION

The width and position of the slits in the Bitter discs shifted according to the presence of internal stresses in the as-received Cu-Ag sheets from which the discs had been manufactured. We speculated that out-of-plane internal stresses may have produced warping. In-plane stresses, we observed, did indeed result in anisotropy in both the microstructure and the mechanical properties of the as-received sheets [27]. We found that, even from a sheet with both internal stresses and warping, it was possible to make a disc that met specifications with respect to slit size and position, as long as the slit was correctly aligned, i.e., more or less perpendicular to the original rolling direction of the sheet (Fig. 5). (Note, this alignment angle applied only to materials with the macro internal stresses specified in our measurements.)

Our Cu-Ag sheets had <112>{110} texture [27], [28]. This texture indicates that <112> was parallel to the rolling direction of the sheets. In this direction, lattice distortion in microscale was relatively small, but in the direction perpendicular to <112>, lattice distortion was large. Within the Cu ribbons characteristic of our sheets, the lattice parameter was larger than would be found in bulk Cu. Within the Ag ribbons, however, the lattice parameter was smaller than would be found in bulk Ag. We speculate that this lattice distortion may have caused some of the internal stresses that would otherwise have been minimized in our as-received Cu-Ag sheets. In macroscale, therefore, lattice distortion perpendicular to <112> may have been smaller than in the rolling direction, so we were still able to make some slits that met our specification, despite the presence of both warping and anisotropy.

Leaving aside the question of warping, the measured internal stress in as-received sheets was relatively small. Once we took warping into account, however, we found that the internal stress of discs with slits of large distortions matched the measured internal stress of the sheets from which they were fabricated. In previous studies, we observed that internal stresses in Cu-Ag composites could be relieved by either cyclic loading or heat treatment [22], [29], [30]. In addition, warping could be corrected by an engineered deformation method. Thus, we assume that both the internal stress and the warping of high-strength Cu-Ag sheets can be minimized by thermo-mechanical processing.

## V. CONCLUSION

In our high-strength Cu-Ag sheets, we observed frequent warping as well as anisotropy of internal stresses. We attributed both to the anisotropy in the microstructure and in the mechanical properties that was often present in these sheets. A combination of internal stress and warping in the original sheets was reflected in some of our resulting Bitter discs, causing distortion in overall disc geometry and in the sizes and locations of slits and holes.

## ACKNOWLEDGMENT

The authors would like to thank Jack Toth for discussion, Robert Goddard for microstructure examination, and Mary Tyler for editing.

## REFERENCES


[1] J. Toth, M. D. Bird, S. Bole, and J. W. O'Reilly, "Fabrication and assembly of the NHMFL 25 T resistive split magnet," *IEEE Trans. Appl. Supercond.*, vol. 22, no. 3, Jun. 2012, Art. no. 4301604.

[2] J. Toth and S. Bole, "Conceptual design for a next generation resistive large bore magnet at the NHMFL," *IEEE Trans. Appl. Supercond.*, vol. 30, no. 4, Jun. 2020, Art. no. 4300104.

[3] J. Toth and S. T. Bole, "Design, construction, and first testing of a 41.5 T all-resistive magnet at the NHMFL in Tallahassee," *IEEE Trans. Appl. Supercond.*, vol. 28, no. 3, Apr. 2018, Art. no. 4300104.

[4] K. Han et al., "High strength conductors and structural materials for high field magnets," *MRS Adv.*, vol. 1, no. 17, pp. 1233–1239, 2016.

[5] K. Han et al., "Material issues in the 100 T non-destructive magnet," *IEEE Trans. Appl. Supercond.*, vol. 10, no. 1, pp. 1277–1280, Mar. 2000.

[6] K. Han et al., "Bending behavior of high-strength conductor," *IEEE Trans. Appl. Supercond.*, vol. 26, no. 4, Jun. 2016, Art. no. 8400804.

[7] K. Han et al., "Cold-deformed Cu-Ag and Cu-Nb composites," *Ultrafine Grained Materials III (as held at the 2003 TMS Annual Meeting)*, 2003, pp. 273–278.

[8] K. Han et al., "Internal stresses in cold-deformed Cu-Ag and Cu-Nb wires," *Philos. Mag.*, vol. 84, no. 24, pp. 2579–2593, Aug. 2004.

[9] K. Han, V. J. Toplosky, R. Walsh, C. Swenson, B. Lesch, and V. I. Pantsyrnyi, "Properties of high strength Cu-Nb conductor for pulsed magnet applications," *IEEE Trans. Appl. Supercond.*, vol. 12, no. 1, pp. 1176–1180, Mar. 2002.

[10] A. Ishmaku and K. Han, "Characterization of cold-rolled Cu-Nb composite," *Mater. Sci. Forum*, vol. 453, pp. 479–484, 2004.

[11] Y. Leprince-Wang et al., "Microstructure in Cu-Nb microcomposites," *Mater. Sci. Eng. A-Struct. Mater. Properties Microstructure Process.*, vol. 351, no. 1/2, pp. 214–223, Jun. 2003.

[12] B. An et al., "Hardening Cu-Ag composite by doping with Sc," *Mater. Lett.*, vol. 252, pp. 207–210, 2019.

[13] B. L. An et al., "Nucleation and growth of discontinuous precipitates in Cu-Ag alloys," *Mater. Res. Exp.*, vol. 9, no. 2, Feb. 2022, Art. no. 026530.

[14] G. M. Li et al., "Influence of high magnetic field on as-cast structure of Cu-25wt%Ag alloys," *China Foundry*, vol. 10, no. 3, pp. 162–166, May 2013.

[15] L. Qu et al., "Studies of electrical resistivity of an annealed Cu-Fe composite," *J. Appl. Phys.*, vol. 113, no. 17, May 2013, Art. no. 173708.

[16] C. Zhao et al., "Improvement of properties in Cu–Ag composites by doping induced microstructural refinement," *Mater. Sci. Eng.: A*, vol. 799, 2021, Art. no. 140091.

[17] C. C. Zhao et al., "Strength of Cu-28 wt%Ag composite solidified under high magnetic field followed by cold drawing," *Met. Mater. Int.*, vol. 23, no. 2, pp. 369–377, Mar. 2017.

[18] C. C. Zhao et al., "Simultaneously increasing strength and electrical conductivity in nanostructured Cu-Ag composite," *Mater. Sci. Eng. A-Struct. Mater. Properties Microstructure Process.*, vol. 652, pp. 296–304, Jan. 2016.

[19] X. W. Zuo et al., "Microstructure and properties of Cu-6wt% Ag composite thermomechanical-processed after directionally solidifying with magnetic field," *J. Alloys Compounds*, vol. 676, pp. 46–53, Aug. 2016.

[20] L. P. Deng et al., "Hardness, electrical resistivity, and modeling of in situ Cu-Nb microcomposites," *J. Alloys Compounds*, vol. 602, pp. 331–338, Jul. 2014.

[21] L. P. Deng et al., "Thermal stability of Cu-Nb microcomposite wires," *Acta Materialia*, vol. 101, pp. 181–188, Dec. 2015.

[22] K. Han et al., *Fabrication Routes for High Strength High Conductivity Wires*. Santa Fe, NM, USA: Los Alamos Nat. Lab., 1998.

[23] K. Han, J. P. Hirth, and J. D. Embury, "Modeling the formation of twins and stacking faults in the Ag-Cu system," *Acta Materialia*, vol. 49, no. 9, pp. 1537–1540, May 2001.

[24] X. W. Zuo et al., "Microstructural dependence of magnetoresistance in CuAg alloy solidified with high magnetic field," *J. Mater. Process. Technol.*, vol. 224, pp. 208–212, Oct. 2015.

[25] X. W. Zuo et al., "Microstructure evolution of the proeutectic Cu dendrites in diamagnetic Cu-Ag alloys by electromagnetic suppressing convection," *J. Low Temp. Phys.*, vol. 170, no. 5/6, pp. 409–417, Mar. 2013.

[26] *Standard Test Method for Determining Residual Stresses by the Hole-drilling Strain-Gage Method*, A. S. E. 837–94, ASTM, West Conshohocken, PA, USA, 1994.

[27] C. Davy et al., "Fabrication and characterization of nanostructured CuAg (Ag-40at% Cu)," *Microsc. Microanalysis*, vol. 11, no. S02, 2005, Art. no. 1718.

[28] C. A. Davy, K. Han, P. N. Kalu, and S. T. Bole, "Examinations of Cu-Ag composite conductors in sheet forms," *IEEE Trans. Appl. Supercond.*, vol. 18, no. 2, pp. 560–563, Jun. 2008.

[29] K. Han et al., "The fabrication, properties and microstructure of Cu–Ag and Cu–Nb composite conductors," *Mater. Sci. Eng.: A*, vol. 267, no. 1, pp. 99–114, 1999.

[30] K. Han, V. J. Toplosky, R. Goddard, J. Lu, R. Niu, and J. Chen, "Impacts of heat treatment on properties and microstructure of Cu16at% Ag conductors," *IEEE Trans. Appl. Supercond.*, vol. 22, no. 3, Jun. 2012, Art. no. 6900204.